J. Fluid Mech. (1981), *vol.* 106, *pp.* 417–433
Printed in Great Britain

On the stability and flow reversal of an asymmetrically heated open convection loop

By HAIM H. BAU† AND K. E. TORRANCE
Sibley School of Mechanical and Aerospace Engineering,
Cornell University, Ithaca, New York 14853

(Received 29 April 1980 and in revised form 9 December 1980)

Experimental results are reported for a U-shaped, free convection loop. The top of the loop is open to an isothermal reservoir. The horizontal leg and one vertical leg are heated at rates Q_1 and Q_2, respectively. The loop is filled either with water or a water-saturated porous medium. Symmetric heating and asymmetric heating favouring the ascending leg of the loop both yield stable flows. Asymmetric heating favouring the descending leg leads to stable flows when the ratio Q_1/Q_2 is above a critical value. Below this critical value, the flow is observed to oscillate with increasing amplitude until the direction of flow in the loop undergoes a reversal. A steady flow follows the reversal. Analytical results include a stability analysis and time-dependent, one-dimensional numerical calculations, both of which compare favourably with experiment.

The disturbance amplification mechanism is explained in terms of thermal anomalies which move through the loop with the material motion of the fluid. Since the heating and buoyancy generation processes are in phase in the heated, descending leg, a thermal anomaly can amplify as it flows through that leg. As the anomaly moves through the ascending leg, it initiates a subsequent anomaly of opposite sign in the descending leg. The result is an oscillating flow which, under appropriate conditions, can amplify.

1. Introduction

Free convection loops provide a means for circulating fluid without the use of pumps. Such loops are of interest for solar heaters, emergency reactor-core cooling, and process industries. They are also of interest for the understanding of warm springs, seawater circulations in the oceanic crust, and the formation of ore deposits. The circulating flows display a wide range of unstable behaviour. The present paper examines one time-dependent mode, an oscillatory flow which can develop and lead to a flow reversal when a single-phase free convection loop is heated asymmetrically.

Three loop geometries are sketched in figure 1. Circulations through the loops are maintained by the appropriate use of heaters (H) and coolers (C). Also shown are representative flow-rate transients which illustrate an unstable or oscillatory mode in each geometry. Prior studies have examined open loops (figure 1*a*) and closed loops (figure 1*b*). In this paper we consider a third type of loop (figure 1*c*), consisting of a

† Present address: Department of Mechanical Engineering and Applied Mechanics, 111 Towne Building D3, University of Pennsylvania, Philadelphia, Pennsylvania, 19104.

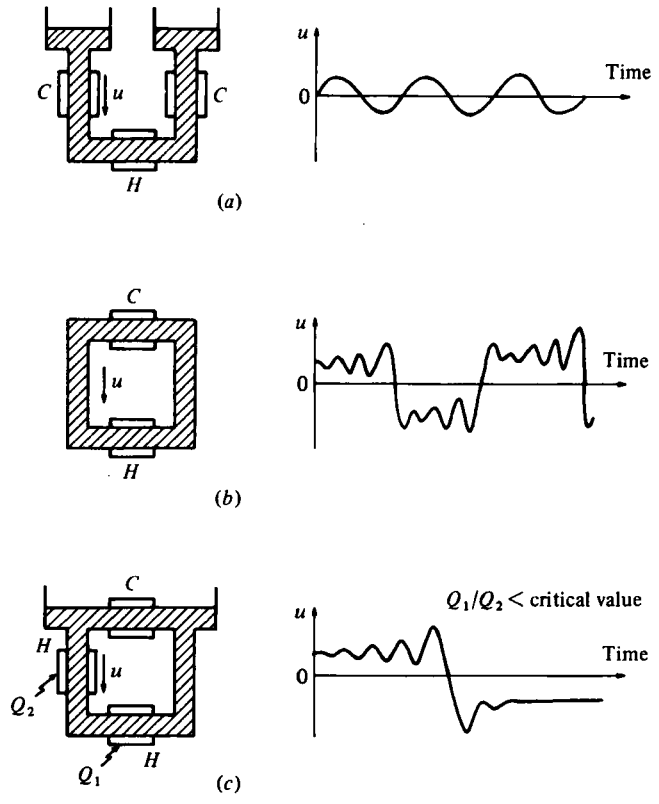

FIGURE 1. Three different free convection loops with heaters (H) and coolers (C). Representative velocity transients (u) are shown at the right. (a) Open loop; (b) closed loop; (c) present study. The present study employs an open loop with a single, isothermal reservoir at the top.

vertical U-tube connected at the top to an isothermal reservoir. Technically this is also an open loop, but with equal inlet and outlet pressures. Such a geometry is representative of a crustal aquifer connected to a single large reservoir. Conditions in such a reservoir (i.e. temperature and pressure) are independent of the aquifer.

Open loops have been considered by Welander (1957) and Martin (1970). Welander's open loop is shown in figure 1 (a), and consists of two reservoirs of finite capacity which are connected by a U-tube. A thermally induced flow leads to pumping from one reservoir to the other. The flow slows down as the reservoir above the rising leg fills. The increasing head ultimately leads to a flow reversal. The resulting flow in the loop is oscillatory, as shown, and is a thermally driven 'sloshing' from one reservoir to the other. Welander presented an approximate criterion for the onset of motion (and thus oscillations) for the case of symmetric heating. Results for asymmetric heating are not available but it is likely that oscillations would exist.

Closed loops have been examined by Keller (1966), Welander (1967), Creveling *et al.* (1975), Damerell & Schoenhals (1979), and others. In a closed loop, figure 1 (b), there is no reservoir interaction. Pressure and temperature vary continuously around the loop. Under certain critical conditions, oscillations are observed to develop and amplify and to lead to a flow reversal. After the reversal the process starts afresh, and the cycle

of reversals continues indefinitely. Welander (1967) presented numerical calculations showing flow reversals, and he also identified and described the instability mechanism. The Welander mechanism allows a thermal anomaly (associated with a fluid parcel) to cycle around the loop and to grow in amplitude with time. As an anomaly moves through the ascending and descending legs, it alternately accelerates or decelerates the flow. This, in turn, couples with a change in the residence time in the subsequent heater or cooler. When favourably coupled, the anomaly amplifies. The amplification mechanism depends on a phase lag between the heating process and the generation of a buoyancy force, and requires an anomaly to cycle continuously around the loop.

Welander formulated his mechanism in terms of a simple loop which was heated from below and cooled from above. The geometry was symmetrical about a vertical plane. Subsequently, Creveling *et al.* (1975) examined experimentally and analytically a symmetrically heated toroidal loop and confirmed the existence of the Welander mechanism. More recently, Damerell & Schoenhals (1979) reported experimental results for an asymmetrically heated toroidal loop. Oscillating flows with continuing reversals were observed when the heating was symmetric or nearly symmetric. For other conditions, one-time, episodic flow reversals occurred when the heating favoured the descending leg. The experiments of Damerell & Schoenhals appear to suggest two instability mechanisms, one associated with symmetric heating (the Welander mechanism) and the other associated with asymmetric heating. The instability mechanism for the latter was not described.

The present paper examines the loop sketched in figure 1 (*c*). The horizontal leg and one of the vertical legs are heated at rates Q_1 and Q_2, respectively. The loop is filled either with water or a water-saturated porous medium. We refer to the two cases as the 'water loop' and the 'porous loop', respectively. Since the loop employs a single isothermal reservoir for supply and discharge, this automatically precludes the oscillatory, sloshing flows described by Welander (1957) for an open loop (see figure 1 *a*). Such flows require separate supply and discharge reservoirs. The present loop also precludes the oscillatory flows with continuing reversals which have been observed for closed loops with symmetric heating (see figure 1 *b*). Since the inlet temperature to the present loop is held constant, it is not possible for thermal disturbances to cycle completely around the loop. The Welander (1967) mechanism can therefore not work. Indeed, symmetric heating of the present loop always leads to stable flows (Bau & Torrance 1981).

On the other hand, asymmetric heating of the present loop (figure 1 *c*) can lead to an instability. The instability occurs when the descending leg is heated preferentially and the heating ratio Q_1/Q_2 is below a critical value. Under such conditions, oscillations in the flow rate are observed to develop and amplify, and to lead to a flow reversal. The transient is sketched in figure 1 (*c*). The flow in the reverse direction is observed to be stable. The instability thus leads to a one-time, episodic flow reversal. This instability is uniquely associated with the asymmetric heating, and is the only single-phase instability observed in the present loop. For the case of closed loops, the asymmetric-heating instability can act in addition to the Welander mechanism.

The following sections describe the experimental apparatus (§ 2), the governing equations (§ 3), the experimental results (§ 4), a linear stability analysis (§ 5), and a finite-amplitude numerical calculation (§ 6). Finally, a discussion of the oscillatory flows, in terms of a simple physical model, is presented (§ 7).

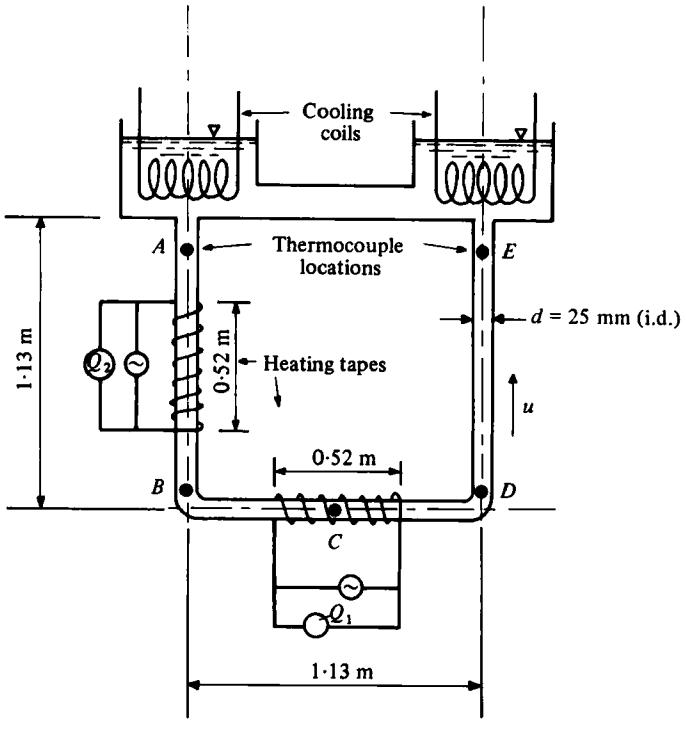

FIGURE 2. The experimental apparatus.

2. Experimental apparatus

A schematic diagram of the free convection loop used for the experiments is shown in figure 2. The open loop is made of Pyrex glass tubing (25 mm inside diameter; 37 mm outside diameter) in the form of three straight segments and two els (70 mm radius of curvature). Each vertical leg is connected at the top to a 30 litre tank, which is open to the atmosphere. The tanks are interconnected by piping of low resistance and are cooled by passing tap water through copper cooling coils.

Heating is accomplished by wrapping the lower horizontal leg and the left vertical leg with nichrome heating tape. The heating is distributed uniformly over the lengths shown in figure 2. The U-shaped loop is insulated with a layer of foil-covered fibreglass insulation. The input heat flux ranges from 0 to 2300 watts for each heating section and is obtained from the heater resistance and the voltage input. Heat losses through the insulation are subtracted to obtain the heat inputs reported in this paper.

Temperatures within the loop were measured with 36 gauge copper–constantan thermocouples located at stations A to E in figure 2. At stations A and E five thermocouples are distributed over the cross-section to obtain an average fluid temperature. Additional single thermocouples are located along the loop (as shown) and in the tanks at the top.

Experiments are conducted either with distilled water in the loop and tanks, or with a non-fluidizing porous medium in the loop. In the latter case, the loop and tanks are also filled with distilled water. The porous medium consists of closely packed, uniformly sized, 5 mm Pyrex beads.

Flow rates in the loop are inferred from the corrected input heat fluxes and the temperature difference between stations E and A (figure 2). During the experiments, the reservoirs at the top were found to remain isothermal with essentially no elevation difference between their free surfaces.

3. Governing equations

To simplify the analysis, we approximate the experimental loop in figure 2 by three straight tubes sequentially arranged in a U shape. Each tube is of internal diameter d and length b. The height and total length L of the loop thus become b and $3b$, respectively. Furthermore, the governing equations are written in a one-dimensional, time-dependent form. This form employs the Boussinesq approximation, assumes constant properties, and is suitable for a loop filled with fluid or a fluid-saturated porous medium. The velocities and temperatures which appear are cross-sectionally averaged values.

For an incompressible fluid, the continuity equation implies that the velocity ($\hat{u}$) is constant within the loop and a function only of time ($\hat{t}$):

$$\hat{u} = \hat{u}(\hat{t}). \tag{1}$$

Carets denote the dimensional form of variables which will later be made non-dimensional. A momentum balance at any axial station $\hat{s}$ along the loop yields

$$\frac{1}{\phi}\frac{\partial \hat{u}}{\partial \hat{t}} + f\frac{\hat{u}^2}{2\hat{d}} + g(1-\beta_f(\hat{T}-T_0))\cos\theta = -\frac{1}{\rho_f}\frac{\partial P}{\partial \hat{s}}, \tag{2}$$

where the various terms are respectively due to inertia, friction, body and pressure forces. In (2), ϕ is the volume porosity, f is the friction factor, g is the acceleration of gravity, β_f is the volume thermal expansion coefficient of the fluid, $\hat{T}(\hat{s})$ is the fluid temperature at station $\hat{s}$, T_0 is a reference temperature (the inlet temperature), θ is the angle between the fluid velocity vector and the vertical, ρ_f is the fluid density at temperature T_0, and P is the pressure. Integration of (2) from inlet to outlet along the loop yields an integral force balance on the fluid in the loop,

$$\frac{1}{\phi}\frac{\partial \hat{u}}{\partial \hat{t}} + f\frac{\hat{u}^2}{2\hat{d}} = \frac{g\beta_f}{L}\int_0^L \hat{T}\cos\theta\, d\hat{s}. \tag{3}$$

The friction factor is expressed in the form

$$f = p/Re^n, \tag{4}$$

where p and n are constants. The Reynolds number is defined in terms of the mean velocity by $Re = \hat{u}d/\nu_f$, where ν_f is the kinematic viscosity of the fluid. Conventional correlations for isothermal flow in a straight pipe lead to $p = 64$ and $n = 1$ for laminar flow, to $p = 0{\cdot}316$ and $n = 0{\cdot}25$ for turbulent flow, and to $p = 2d^2/\lambda$ and $n = 1$ for flow through a porous medium, where λ is the formation permeability (Eckert & Drake 1972, p. 370; Bear 1972, pp. 133, 148 and 166). The foregoing correlations neglect secondary flows due to curvature or buoyancy.

A local heat balance on the loop, neglecting axial conduction and viscous heating, yields

$$r\frac{\partial \hat{T}}{\partial \hat{t}} + \hat{u}\frac{\partial \hat{T}}{\partial \hat{s}} = \begin{cases} \dfrac{4\hat{Q}_i}{\pi d^2 b_i \rho_f c_{pf}} & \text{in heater sections } i = 1 \text{ or } 2, \\ 0 & \text{otherwise,} \end{cases} \tag{5}$$

where $\hat{Q}_i$ is the heat input in either heated section, b_i is the appropriate heater length, c_p is the specific heat, and r is a ratio of volumetric heat capacities given by

$$r = \frac{\phi\rho_f c_{pf} + (1-\phi)\rho_m c_{pm}}{\rho_f c_{pf}}. \tag{6}$$

Subscripts f and m respectively denote the fluid and the solid matrix appearing in the porous loop. For the porous loop, $\phi = 0{\cdot}44$ and $r = 0{\cdot}72$. For the water loop, we have $\phi = 1$ and $r = 1$.

We next introduce non-dimensional variables:

$$s = \frac{\hat{s}}{b}, \quad t = \left(\frac{8Q_2}{\pi}\right)^{\frac{1}{3}} \frac{\nu_f}{bd}\hat{t}, \quad u = \left(\frac{\pi}{8Q_2}\right)^{\frac{1}{3}} \frac{d}{\nu_f}\hat{u},$$

$$T = \frac{1}{2}\left(\frac{\pi}{Q_2}\right)^{\frac{2}{3}} \frac{b}{L}\frac{g\beta_f d^3}{\nu_f^2}(\hat{T} - T_0), \quad Q_2 = \frac{b}{L}\frac{g\beta_f d^2}{\rho_f c_{pf}\nu_f^3}\hat{Q}_2, \tag{7}$$

and

$$Y = \frac{Q_1}{Q_2}, \quad f = \frac{m}{u^n}, \quad m = p\left(\frac{\pi}{8Q_2}\right)^{\frac{1}{3}n}. \tag{8}$$

Q_1 and Q_2 denote the rates of heat addition to the horizontal and vertical legs, respectively. Substitution of (7) and (8) into the momentum and energy equations yields

$$\left(\frac{2d}{\phi b}\right)\frac{\partial u}{\partial t} + mu^{2-n} = \int_0^{L/b} T\cos\theta\, ds, \tag{9}$$

$$r\frac{\partial T}{\partial t} + u\frac{\partial T}{\partial s} = \begin{cases} b/b_2 & \text{in the vertical heater,} \\ bY/b_1 & \text{in the horizontal heater,} \\ 0 & \text{otherwise.} \end{cases} \tag{10}$$

In the above, four geometric parameters from the loop appear: d/b, L/b, b/b_1, and b/b_2. The scaling quantities were selected to avoid introducing a separate buoyancy parameter in (9).

Without loss of generality in the subsequent analyses, we shall assume that heating is uniformly distributed over the length of each heated leg ($b/b_1 = b/b_2 = 1$). The steady-state solution (subscript s) for flow in the counter-clockwise sense in figure 2 is

$$u_s = \left(\frac{1+2Y}{2m}\right)^{1/(3-n)}, \tag{11}$$

$$T_s = \begin{cases} s/u_s & \text{in section } AB \quad (0 \leqslant s < 1), \\ \{1 + Y(s-1)\}/u_s & \text{in section } BD \quad (1 \leqslant s < 2), \\ (1+Y)/u_s & \text{in section } DE \quad (2 \leqslant s \leqslant 3). \end{cases} \tag{12}$$

The equations governing the steady state also admit a solution corresponding to flow in the clockwise sense. The two flows correspond to descending and ascending flow, respectively, through the vertical heater. Since the buoyant drives for the two flows are the same, their velocities are identical and are given by (11). At first glance it may appear that the two flows should be equally stable. For example, a positive perturbation of the steady-state velocity generally leads to a reduced total buoyancy and an increased frictional drag. Both effects serve to damp the perturbation and to return

the flow to the original steady state. In spite of this argument, the experimental results in the next section show that the two directions of flow are not equally stable. To explain the instability, it is necessary to carry out a transient stability analysis (§ 5) based on the time-dependent equations (9) and (10).

4. Experimental results

When a specified amount of heat Q_1 is supplied to the horizontal leg of the loop, and no heat is added to the vertical leg (i.e. $Q_2 = 0$), flows are observed to develop in either direction through the loop with equal probability. The transients and the resulting steady flows have been described by Bau & Torrance (1981). Their stability analyses show that the rest state is always unstable (i.e. the critical Rayleigh number for the onset of motion is zero), and that the steady-state motion for such symmetric heating is stable.

The present experiments examine the influence of adding heat Q_2 to the vertical leg while simultaneously heating the horizontal leg. Heating is thus asymmetric. When heat is added to an ascending flow in the vertical leg (i.e. clockwise motion in figure 2), we observe that the resulting motion is stable. When heat is added to a descending flow in the vertical leg (i.e. counter-clockwise motion), the resulting flow may start to oscillate. The nature and onset of the oscillations will now be described. The discussion is centred on the porous loop, but results are similar for the water loop.

A counter-clockwise flow may be established in the loop by low-level preheating of the right (ascending) leg and by supplying a specified amount of heat Q_1 to the horizontal leg. The heat supply Q_2 to the left (descending) leg is then increased in a sequence of small steps. After each step sufficient time is allowed for transient effects to die out. During the transient the flow at first decelerates because the immediate effect of the incremental heating is to reduce the buoyant drive. However, after a time lag (needed for the warmer fluid to reach the ascending leg) the flow accelerates to a new steady state. Steady-state results for the porous loop are shown in figure 3 in terms of the temperature difference across the horizontal leg, $\Delta\hat{T}_{DB} = \hat{T}_D - \hat{T}_B$, and the temperature difference across the loop, $\Delta\hat{T}_{EA} = \hat{T}_E - \hat{T}_A$. The abscissa is $\hat{Q}_2$ while $\hat{Q}_1$ is held fixed. All variables are dimensional. The decrease in $\Delta\hat{T}_{DB}$ with increasing $\hat{Q}_2$ indicates an increase in the flow rate $\hat{u}$ through the loop (the product $\hat{u}\Delta\hat{T}_{DB}$ remains constant when $\hat{Q}_1$ is fixed). On the other hand, the increase in $\Delta\hat{T}_{EA}$ indicates an increasing heat content at discharge (the product $\hat{u}\Delta\hat{T}_{EA}$ is proportional to $\hat{Q}_1 + \hat{Q}_2$).

For $\hat{Q}_2$ greater than 55 watts a steady state was not achieved. Instead, the flow strated to oscillate. An example of an oscillating flow is shown in figure 4. This figure illustrates $\Delta\hat{T}_{EA}$ and the temperature difference between the centre of the horizontal leg and the inlet, $\hat{T}_{CO} = \hat{T}_C - \hat{T}_0$. For counter-clockwise flow the inlet is located at station A in figure 2. The period of the oscillations in figure 4 is about twice the flow time through the loop. The oscillations amplify until the flow reverses direction. The reversed flow corresponds to an ascending motion in the heated vertical leg and is stable after the disturbances damp out. In the porous loop, time intervals as long as 36 hours were observed between the start of oscillations and an ensuing flow reversal.

Clearly, oscillations develop when a critical value of the ratio $Y = \hat{Q}_1/\hat{Q}_2$ is attained. The growth rate of the oscillations increases as Y is decreased below the critical value.

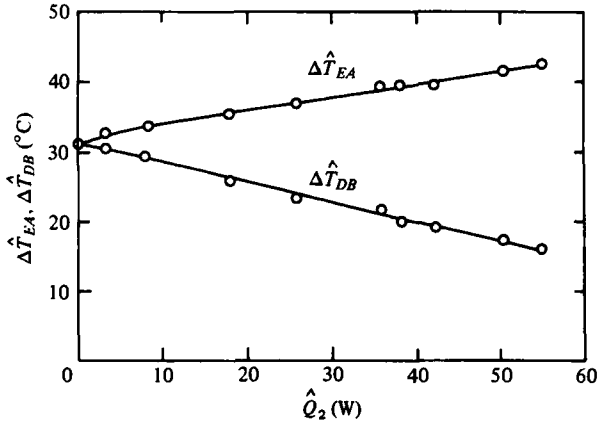

FIGURE 3. Experimentally measured temperature differences between outlet and inlet, $\Delta\hat{T}_{EA}$, and across the heater, $\Delta\hat{T}_{DB}$, in the porous loop as a function of the heating rate in the descending leg, $\hat{Q}_2$. The heating rate in the horizontal leg is constant at $\hat{Q}_1 = 42$ watts.

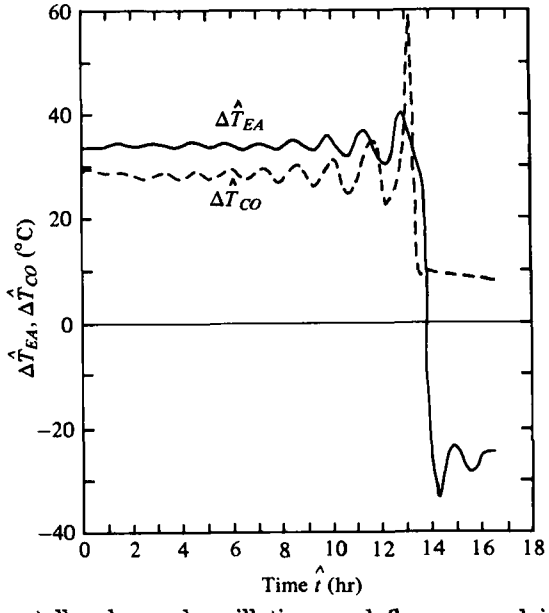

FIGURE 4. Experimentally observed oscillations and flow reversal in the porous loop. The temperature difference between outlet and inlet, $\Delta\hat{T}_{EA}$, and between the centre of the heater and the inlet, $\Delta\hat{T}_{CO}$, are shown for a heating ratio of $Y = \hat{Q}_1/\hat{Q}_2 = 0{\cdot}618$ with $\hat{Q}_1 = 27{\cdot}5$ watts and $\hat{Q}_2 = 44{\cdot}5$ watts.

Values of Y are given in tables 1 and 2 for the porous loop and the water loop, respectively. The Y-values correspond to the last stable flow before the onset of oscillations.

Also shown in the tables, as approriate, are the Reynolds number, $Re = \hat{u}d/\nu_f$, the ratio of a modified Grashof number to the Reynolds number, Gr^*/Re, and the oscillation period of the first unstable flow. The velocity $\hat{u}$ in the Reynolds number is found from

$\hat{Q}_2$(W)	$Y = \hat{Q}_1/\hat{Q}_2$	Re	Oscillation period (hours)
18·6	0·86	19·2	1·7
44·5	0·65	33·6	1·4
55·0	0·76	38·4	1·0
85·0	0·68	45·0	1·0
121·0	0·75	60·0	0·9

TABLE 1. Experimentally determined values of Y, Re, and the oscillation period at the onset of oscillations in the porous loop.

$\hat{Q}_2$(W)	$Y = \hat{Q}_1/\hat{Q}_2$	Re	Gr^*/Re
84·9	0·195	303	7750
106·4	0·184	368	8000
220·0	0·058	484	12600
415·0	0·083	567	20200
445·0	0·128	489	25100
666·0	0·084	768	24000

TABLE 2. Experimentally determined values of Y, Re, and Gr^*/Re at the onset of oscillations in the water loop.

the measured values of $\Delta\hat{T}_{EA}$ and $\hat{Q}_1+\hat{Q}_2$ by using a global heat balance (found by integrating (5)):

$$\hat{u} = \frac{4(\hat{Q}_1+\hat{Q}_2)}{\pi d^2 \rho_f c_{pf} \Delta\hat{T}_{EA}}. \tag{13}$$

All fluid properties are evaluated at the mean temperature of the fluid in the loop. The ratio Gr^*/Re will be useful in a later discussion and is defined by

$$\frac{Gr^*}{Re} = \frac{g\beta_f d^3 q_2}{k\nu_f \hat{u}}, \tag{14}$$

where q_2 is the heat flux (per unit surface area) in the vertical leg and k is the thermal conductivity of the medium within the loop.

5. Stability analysis

In this section we shall show that the transient, one-dimensional equations (§ 3) are capable of predicting the instabilities which were observed experimentally (§ 4). A linear stability analysis is applied which yields the necessary conditions for the onset of instability.

We first introduce a small perturbation of the steady state of the form

$$u = u_s + u' \quad \text{and} \quad T = T_s + T', \tag{15}$$

where primes denote the perturbation and all variables are non-dimensional. Substituting (15) into the governing equations (9) and (10), subtracting the steady-state solution (11) and (12), and neglecting terms of second order, we obtain

$$\left(\frac{2d}{\phi b}\right)\frac{\partial u'}{\partial t} + m(2-n)\,u_s^{1-n}u' = \int_0^{L/b} T' \cos\theta\, ds, \tag{16}$$

$$r\frac{\partial T'}{\partial t}+u_s\frac{\partial T'}{\partial s}+u'\frac{\partial T_s}{\partial s}=0. \tag{17}$$

The linearized equations accept a solution of the form

$$u'=\tilde{u}\,e^{\omega^* t},\quad T'=\tilde{T}(s)\,e^{\omega^* t}, \tag{18}$$

where tildes denote the perturbation amplitude and ω^* is the growth rate. We will consider the system unstable if ω^* has a positive real part. After substituting (18) into the energy equation (17), integration yields

$$\tilde{T}=\begin{cases}\dfrac{\tilde{u}}{r\omega^* u_s}\left(e^{-r\omega^* s/u_s}-1\right) & \text{for}\quad 0\leqslant s<1,\\[2ex] \dfrac{\tilde{u}}{r\omega^* u_s}\left\{\left(e^{-r\omega^*/u_s}-1+Y\right)e^{-r\omega^*(s-1)/u_s}-Y\right\} & \text{for}\quad 1\leqslant s<2,\\[2ex] \dfrac{\tilde{u}}{r\omega^* u_s}\left\{\left(e^{-r\omega^*/u_s}-1+Y\right)e^{-r\omega^*/u_s}-Y\right\}e^{-r\omega^*(s-2)/u_s} & \text{for}\quad 2\leqslant s\leqslant 3.\end{cases} \tag{19}$$

Substitution of (19) into the momentum equation (16) yields a characteristic equation for the normalized growth rate $\omega=r\omega^*/u_s$, given by

$$F(\omega)=M+(2-n)\left(\tfrac{1}{2}+Y\right)\omega^{-1}-\omega^{-2}-\left\{e^{-3\omega}+2e^{-2\omega}+Y(e^{-2\omega}+2e^{-\omega}-1)\right\}\omega^{-3}=0, \tag{20}$$

where $M=2du_s^3/\phi br$.

The parameter M is essentially proportional to the fluid inertia. The steady-state velocity u_s from (11) has been used in (20), and may also be used to rewrite M as

$$M=\left\{\frac{2Z}{1+2Y}\right\}^{-3/(3-n)},\quad \text{where}\quad Z=m\left(\frac{\phi br}{2d}\right)^{(3-n)/3}. \tag{21}$$

The governing parameters in the characteristic equation (20) are thus seen to be n, Y and Z. The parameter Z also expresses the importance of the inertia term in (9). Large values of Z occur when m is large or d/b is small. In either case, inertia effects are small and the remaining friction and buoyancy terms in (9) tend to balance. On the other hand, small values of Z imply that inertia effects are important.

The Nyquist criterion (Carrier, Krook & Pearson 1966, p. 61) is applied to investigate whether or not (20) has roots in the ω plane with a positive real part. The Nyquist criterion says, in essence, that the number of roots of (20) within a given closed curve in the ω plane is equal to the number of times $F(\omega)$ encircles the origin in the F plane as ω traverses the given closed curve. $F(\omega)$ must be analytic within, and analytic and non-zero on, the closed curve.

It will be convenient to introduce a translated F-plane given by

$$H(\omega)=F(\omega)-M \tag{22}$$

and which is shown in figure 5. Next, consider the closed curve shown in the insert of figure 5. The curve may be enlarged to include the entire right half of the ω-plane. The enlarged curve is mapped into the H plane as follows: The large semicircle of the closed curve in the insert maps into the origin of the H plane. The small semicircle maps to a half-circle at infinity in the right half of the H plane. The positive imaginary branch of the closed curve in the insert is shown by the solid curves in the H plane for three different values of the heating ratio Y and for $n=1$. The negative imaginary branch

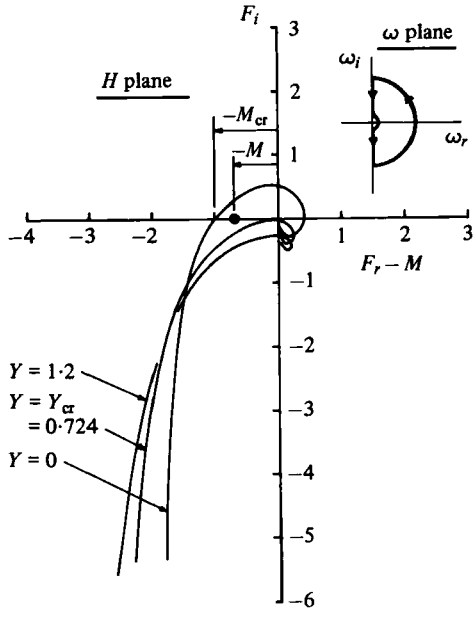

FIGURE 5. Nyquist plot of (20) in the complex plane $H(\omega) = F(\omega) - M$ which illustrates the relationship between the heating ratio Y (the curve parameter) and M for the case $n = 1$. The locations of a point, $-M$, and a critical value, $-M_{cr}$, are shown. The insert shows the integration path to be followed in the ω-plane.

of the closed curve is given by the mirror image (not shown) of the solid curves about the real axis.

For $F(\omega)$ to have roots within the closed contour in the ω plane, the point $-M$ in the H plane must be encircled by the mapped curve. The filled circle in the H-plane illustrates a possible location for the point $-M$. Clearly, there exists a value of $Y = Y_{cr}$ at which the mapped curve is just tangent to the real axis. For $Y > Y_{cr}$, the mapped curve never crosses the real axis. Since a point $-M$ can never be encircled, the system is always stable. For $Y < Y_{cr}$, the mapped curve crosses the real axis and may encircle a point $-M$ as shown for $Y = 0$. The system is thus unstable for a range of values $0 < M < M_{cr}$, and is stable for $M > M_{cr}$. Clearly, M_{cr} depends on Y and n. With Y and n known, (21) may be used to replace M by Z. For $Y < Y_{cr}$, the conditional stability requirement $M > M_{cr}$ is alternatively expressed by Z being less than a critical value.

The procedure illustrated in figure 5 has been extended to a range of values of the friction-law exponent n. The resulting stability diagram is shown in figure 6 with Y as the ordinate and n as the abscissa. The heavy line shows Y_{cr}, which is a function only of n. The curve parameter for the light lines is Z. For $Y > Y_{cr}$, flows are always stable. For $Y < Y_{cr}$, stable flows exist only when Z is less than the value indicated by the curve parameter. Clearly, for a given value of the friction-law exponent n, figure 6 allows zones of stable and unstable flows to be identified.

Figure 7 illustrates a comparison between theory and experiment. The ordinate is Z, the abscissa is Y, and the curve parameter is n. The solid lines denote results from the linearized stability theory (i.e. from figure 6). The crosses and circles respectively represent experimental data from tables 1 and 2 for the porous and water loops. Squares

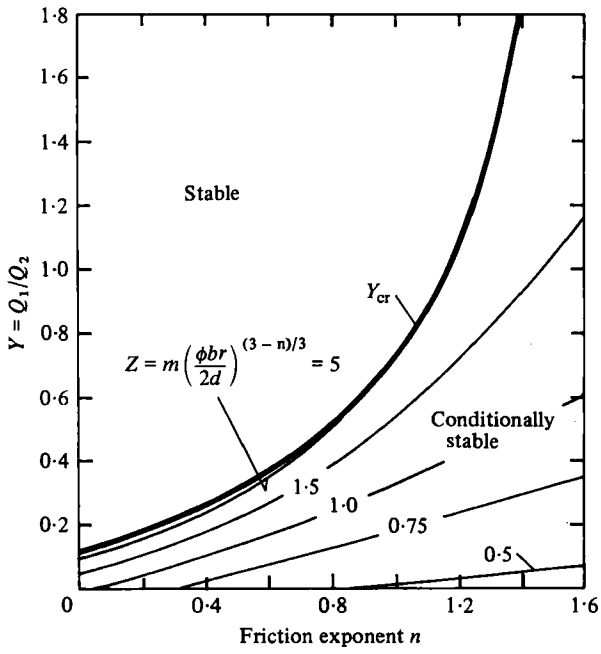

FIGURE 6. Stability diagram based on (20) and (21) which illustrates the relationship between the heating ratio $Y = Q_1/Q_2$, the friction exponent n (from (4)), and the parameter Z. Y-values above and below Y_{cr} correspond, respectively, to stable and conditionally stable flows. For $Y < Y_{cr}$, flows are stable provided Z is less than the critical value shown on the curves.

denote results from a finite-amplitude numerical calculation to be described in the next section. Filled squares denote unstable (oscillatory) flows, while open squares denote stable flows. In preparing figure 7, we have assumed n-values of 1 and 0·25 for the porous and water loops, respectively. The former value corresponds to laminar and Darcy-type flows, whereas the latter corresponds to turbulent flow. Darcy-type flow in the porous loop is supported by the experiments of Bau & Torrance (1981). Turbulent flow in the water loop is suggested by the large values of Gr^*/Re given in table 2. Large values of this ratio indicate that local free convection effects in the descending heated flow are sufficient to trigger the onset of turbulence. A critical value of $Gr^*/Re \approx 520$ for the onset of turbulence has been reported by Scheele & Hanratty (1962) for experiments in tall vertical tubes.

Clearly, there is good agreement in figure 7 between the results of the linear stability analysis and the numerical calculations. Experimental results for both the porous and water loops tend to scatter about the curves based on linear stability theory for $n = 1$ and 0·25, respectively. The mean of the experimental results for the water loop falls somewhat to the left of the linear stability curve for $n = 0{\cdot}25$. This may indicate that local free convection effects within the descending leg lead to n-values less than 0·25 for the water loop. We also note that each set of experimental data points (water loop and porous loop) ranges from low heat flows (upper points) to the onset of boiling (lower points). Experimental data for the porous loop correspond to large values of the ordinate (note break in scale) because m depends inversely on the permeability of the porous medium.

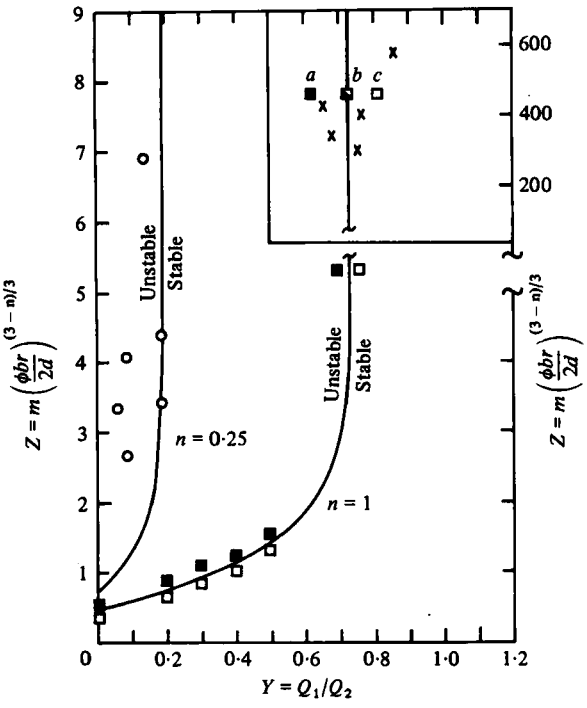

FIGURE 7. Comparison of linear stability theory, experiment, and finite-amplitude numerical calculations. Solid curves illustrate results of the linear stability theory from figure 6 assuming $n = 1$ for the porous loop and $n = 0{\cdot}25$ for the water loop. Experimental results are from tables 1 and 2 and correspond to the last stable flow before the onset of oscillations and flow reversal: ×, porous loop; ○, water loop. Numerical results correspond to: □, stable flow; ◪, neutrally stable flow; ■, unstable flow. Velocity transients at points labelled *a*, *b*, and *c* are shown in figure 9. Note the change of scale used for the insert to display results for the porous loop.

6. Numerical solutions

Numerical solutions of the governing equations have been carried out in order to examine the nature of the instability predicted by linear theory (§ 5), and to compare the subsequent growth of the instability with the oscillations and flow reversal observed in the experiments (§ 4). Calculations were undertaken for a friction law corresponding to laminar flow or to flow in a porous medium (i.e. $n = 1$).

Finite differences were used to approximate (9) and (10). Forward time and backward space differences were used for (10). The momentum equation (9) was approximated using a backward time difference and Simpson's rule for the buoyancy integral. For $n = 1$ both momentum and energy equations could be solved explicitly. Stability of the time advancement requires that the inequality $u\Delta t/r\Delta s \leqslant 1$ be satisfied, where Δt is the time step and Δs is the spatial mesh size (taken as 0·125). The leading truncation error appears in the energy equation, is dissipative, and is proportional to $u\Delta s(1 - u\Delta t/r\Delta s)$. The calculations reported here correspond to values of $u\Delta t/r\Delta s = 0{\cdot}9$. The dissipation introduced into the calculations appears to compensate, at least approximately, for the diffusing effect of secondary flows in the experiments.

Initial conditions for the calculations correspond to the steady-state solution given by (11) and (12). The inlet temperature is maintained at $T = 0$. A disturbance is

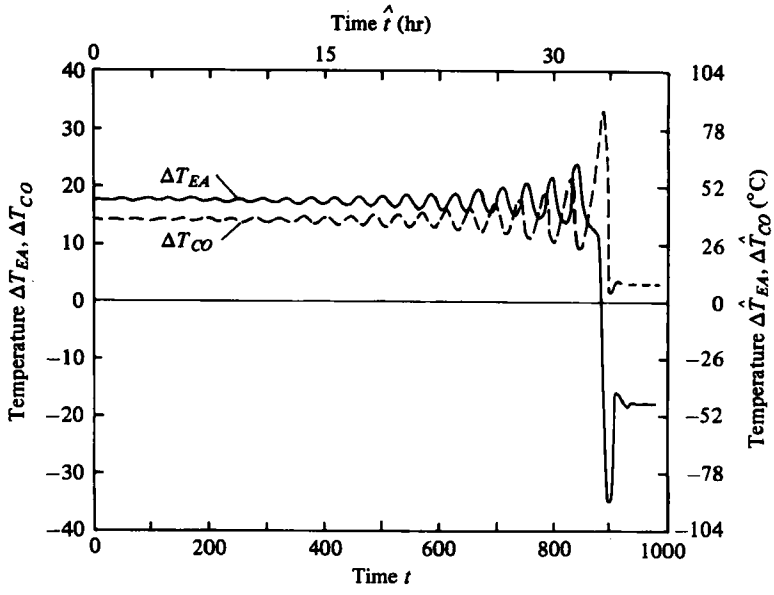

FIGURE 8. Numerically calculated oscillations and flow reversal in the porous loop. The temperature differences ΔT_{EA} and ΔT_{CO} are shown for $Y = 0{\cdot}618$. The left-hand and bottom scales are non-dimensional. The right-hand and top scales are dimensional and allow a comparison with the experimentally measured transients in figure 4.

introduced at $t = 0$ in the velocity field in order to trigger the oscillations. A velocity disturbance of 5 % was used for the unstable cases, and disturbances as large as 30 % for the stable cases. Without the introduction of a disturbance, the flows remained stable.

Calculated transients are shown in figure 8 for conditions corresponding to the experimental results in figure 4. To facilitate comparison, the oridinate and abcissa in figure 8 are shown in both dimensional and non-dimensional form. The zero of the experimental record corresponds to the time at which oscillations were first noted, and thus the very early growth period is not shown. Uncertainties in estimating the heat losses cause the calculated temperatures to fall somewhat higher than the experimental record. In addition, secondary flows and axial conduction in the experiment account for the attenuation of the experimental peaks relative to the computed peaks. Nevertheless, there is a strong resemblance between the calculated and experimental results. Comparisons at other values of Y show similar agreement but are not presented here.

Calculated results are displayed in another way in figure 9. This figure illustrates the velocity in the loop for three different values of Y. The initial perturbation in the velocity at $t = 0$ is amplified, neutrally propagated, or damped, respectively, as Y is less than, equal to, or greater than Y_{cr}. The three cases correspond to the points labelled a, b, and c in figure 7. Numerically determined stability boundaries match those obtained from the linear theory. Representative results are shown in figure 7 along the linear stability curve for $n = 1$.

Temperature distributions within the loop for the disturbance-amplifying case in figure 9 (a) are shown in figure 10. The abscissa is the axial co-ordinate s. The ordinate

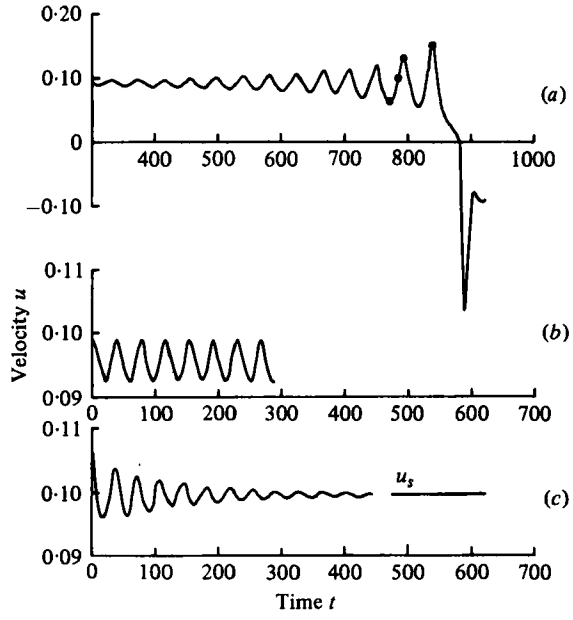

FIGURE 9. Numerically calculated non-dimensional velocities in the loop as a function of non-dimensional time for the points labelled *a*, *b* and *c* in figure 7. (*a*) Unstable flow, with amplifying oscillations which lead to a flow reversal, $Y = 0{\cdot}618$; (*b*) neutrally stable flow, $Y = 0{\cdot}724$; and (*c*) stable flow with damped oscillations, $Y = 0{\cdot}832$.

is the non-dimensional disturbance temperature, $T(s)$, measured relative to the steady state, $T_s(s)$. The four curves correspond to the solid points shown in figure 9(*a*). Times $t = 770$, 780 and 790 respectively correspond to the minimum, intermediate, and maximum velocity in the loop during an accelerating phase. The motion of a heated warm pulse through the loop is clearly visible in the migration of the peak. The distribution at $t = 840$ corresponds to the peak velocity of the subsequent pulse through the loop. The higher temperatures imply a greater buoyancy force, and thus higher velocities. Eventually, the oscillations lead to a flow reversal at $t = 880$.

7. Discussion

The preceding sections outline experimental and analytical evidence for the critical conditions leading to instabilities in an open convection loop of the type shown in figure 2. Symmetric heating, asymmetric heating favouring the ascending flow, and weak asymmetric heating favouring the descending flow, are all stable. When the descending leg is heated to a critical value relative to the horizontal leg, the flow starts to oscillate and eventually reverses.

A physical mechanism for the oscillations and the flow reversal will now be described. Briefly, the mechanism depends on the motion through the loop of fluid parcels with positively or negatively perturbed temperatures (relative to a steady state). Such perturbations could initiate from a small disturbance in either the flow rate or the heating rate. In addition, the mechanism requires asymmetric heating which favours the descending leg of the loop.

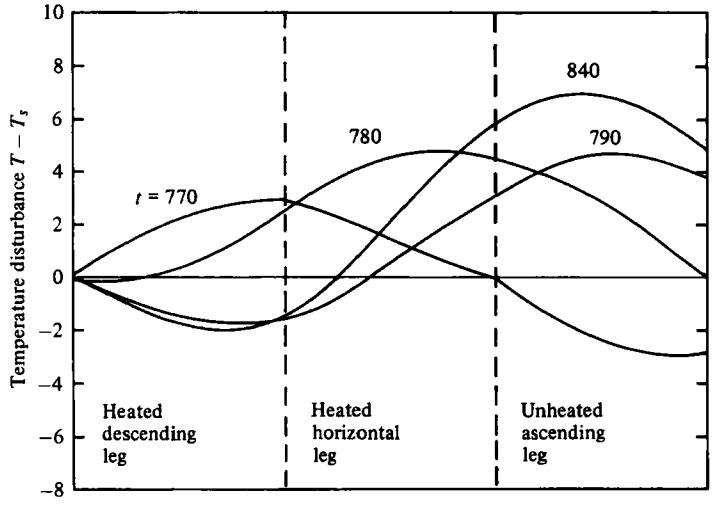

FIGURE 10. Profiles of the temperature disturbance, $T-T_s$, within the loop. $T(s)$ is the instantaneous temperature, $T_s(s)$ is the steady-state temperature given by (12), and the four time levels correspond to the filled circles in figure 9(*a*).

Consider a positive thermal anomaly in the heated, descending leg. Such an anomaly causes a decrease in the total buoyancy. This tends to decelerate the flow, although there may be some inertial lag. Thus, the anomaly tends to move more slowly through the descending leg, receives additional heating, and can be amplified. If the flow is not actually brought to rest the warm pocket will, after a time lag, reach the ascending leg. As it rises in the ascending leg the total buoyancy will increase. The resulting acceleration causes new fluid to proceed through the heated, descending leg more rapidly than normal. This forms a descending cold pocket which can also amplify. When the cold pocket reaches the ascending leg it will, in turn, induce a subsequent warm pocket in the descending leg.

The result is a continuing sequence of thermal anomalies of alternating sign. Each anomaly can amplify while in the descending leg since the heating and buoyancy-generation processes are in phase. The oscillatory period of the flow is about twice the transit time through the loop. This is the period observed in the present experiments and numerical calculations. When the oscillations amplify, the disturbance grows in time until the flow is momentarily brought to rest and a flow reversal follows (see figure 9*a*). The reversed flow is stable because the heating and buoyancy generation processes in the ascending leg serve to damp, rather than amplify, disturbances. Note that the present amplification mechanism differs from the Welander (1967) mechanism for closed loops. The latter depends upon a phase lag between the heating and buoyancy-generation processes, and on the continuous cycling of disturbances around a loop.

The disturbance amplification mechanism allows us to interpret the trends in figure 7 in terms of a balance between buoyancy fluctuations and the damping effects of friction and inertia. At large values of Z (small inertia), the stability curves approach asymptotic values. This corresponds to a region where stability is a result of the damping effect of friction. At lower values of Z the region of stability in figure 7 increases. In this region, fluid inertia causes a slow response in the disturbance

amplification process. At very low values of Z inertia effects dominate and the flows are always stable. This is in contrast to the observations of Damerell & Schoenhals (1979), who never observed a stable region when the descending leg of their closed loop was preferentially heated. This may be because the Welander (1967) mechanism was always present as an additional mechanism in their experiments.

This research was supported by the Division of Engineering of the National Science Foundation of the United States under Grant ENG-7823542.

REFERENCES

BAU, H. & TORRANCE, K. E. 1981 Transient and steady behavior of an open, symmetrically-heated, free convection loop. *Int. J. Heat Mass Transfer* **24**, 597.

BEAR, J. 1972 *Dynamics of Fluids in Porous Media*. Elsevier.

CARRIER, G. F., KROOK, M. & PEARSON, C. E. 1966 *Functions of a Complex Variable – Theory and Techniques*. McGraw-Hill.

CREVELING, H. F., DE PAZ, J. F., BALADI, J. Y. & SCHOENHALS, R. J. 1975 Stability characteristics of a single-phase free convection loop. *J. Fluid Mech.* **67**, 65.

DAMERELL, P. S. & SCHOENHALS, R. J. 1979 Flow in a toroidal thermosyphon with angular displacement of heated and cooled sections. *J. Heat Transfer* **101**, 672.

ECKERT, E. R. G. & DRAKE, R. M. 1972 *Analysis of Heat and Mass Transfer*. McGraw-Hill.

KELLER, J. B. 1966 Periodic oscillations in a model of thermal convection. *J. Fluid Mech.* **26**, 599.

MARTIN, S. 1970 A hydrodynamic curiosity: the salt oscillator. *Geophys. Fluid Dynamics* **1**, 143.

SCHEELE, G. F. & HANRATTY, T. J. 1962 Effects of natural convection on stability of flow in a vertical pipe. *J. Fluid Mech.* **14**, 244.

WELANDER, P. 1957 Note on the self-sustained oscillations of a simple thermal system. *Tellus* **9**, 419.

WELANDER, P. 1967 On the oscillatory instability of a differentially heated fluid loop. *J. Fluid Mech.* **29**, 17.